EGYPTIAN PHARMACEUTICAL JOURNAL EPJ Original article 274

Rosuvastatin loaded bilosomes as an innovative therapeutic approach for radiation-induced cardiovascular alterations by targeting Nrf2/HO-1 pathway

Noha A. Fadel[1], Walaa A. El-Sabbagh[1], Asmaa B. Darwish[2] and Mostafa M. Younis[2]

[1]Drug Radiation Research Department, National Centre for Radiation Research and Technology, Egyptian Atomic Energy Authority (EAEA), Cairo, Egypt.
[2]Pharmaceutical Technology Department, National Research Centre, Dokki, Cairo, Egypt
Correspondence to Noha A. Fadel (PhD)
Drug Radiation Research Department, National Center for Radiation Research and Technology (NCRRT), Egyptian Atomic Energy Authority (EAEA), 11787, Cairo, Egypt.
e-mail: noha_d5@hotmail.com
ORCID: https://orcid.org/0000-0002-8856-2643

Received: 3 November 2024
Revised: 23 November 2024
Accepted: 26 November 2025
Published: 20 March 2025

Egyptian Pharmaceutical Journal 2025, 24: 274-288

Background
The cardiovascular hazards associated with radiotherapy have become a major issue. Statins have been shown to improve the survival rate and hinder the cardiovascular harm in cancer patients exposed to radiotherapy.
Objective
The current study attempted to evaluate the efficacy of rosuvastatin (ROSU) loaded in bilosomes (BLs) drug carrier, as a new formulation to mitigate the cardiovascular deteriorations induced by radiation exposure in experimental rats.
Materials and methods
Rosuvastatin loaded bilosomes (ROSU-BLs) were prepared using the thin film hydration technique. Characterization of the prepared formulations was performed by several approaches. The in vitro release profile was carried out using the dialysis bag diffusion technique. In the experimental in vivo phase, rats were exposed to γ-radiation (7 Gy) and treated with ROSU either free or formulated form to evaluate their redox, anti-hyperlipidemic, anti-inflammatory and anti-apoptotic activities.
Results and conclusion
The results revealed the efficient development of ROSU-BLs, which exhibited entrapment efficiency (EE%) varying from 65.47% to 86.87%, particle sizes in nanosized range from 247.4 to 414 nm, negatively charged zeta potential and transmission electron microscopy (TEM) verified the conventional sphere-shaped vesicles. In vitro release study revealed biphasic pattern with extended release of ROSU up to 24 h. In vivo results showed the advantage of ROSU-BLs compared to free ROSU in enhancing cardiac redox activity by restoring the nuclear factor erythroid 2-related factor 2 (Nrf2) and heme oxygenase-1 (HO-1) levels, while concurrently diminishing the levels of tumor necrosis factor-alpha (TNF-α) and caspase-9 in cardiac tissue. Such impact was also verified by histopathological investigations. In conclusion, the current data indicate the efficacy of bilosomes carrier in improving the oral delivery of ROSU, reflected by the enhanced potential of ROSU-BLs to mitigate the cardiovascular deteriorations induced by γ-radiation via activating the cardiac redox Nrf2/HO-1 system with consequent suppression of pro-inflammatory and pro-apoptotic markers.

Keywords: Rosuvastatin, bilosomes, radiation, cardiovascular, redox
Egypt PharmaceutJ 24:274–288

1687-4315

Introduction

Although radiation therapy is widely used as a part of cancer treatment protocol, it still carries numerous adverse cardiovascular complications in patients receiving radiation therapy in the thoracic and chest areas as shown in breast, lung, and esophageal cancer patients [1-3]. Radiation therapy could induce damage to any part of the heart tissue, in addition to the high incidence of atherosclerosis [4]. The cardiac damage and susceptibility to ischemic heart disease are proportional to the radiation dosage level, frequency, and exposed heart area [5]. For instance, studies showed that breast cancer patients receiving radiation therapy for the left breast were having more cardiac complications than patients with right breast cancer [6]. Research generally indicates that for every gray (Gy) of radiation exposure, there was a substantial 3% increase in the risk of cardiac death [5].

Several hypotheses have been brought on to explain how exposure to radiation causes cardiovascular diseases, with oxidative stress serving as the primary driver of

these hypotheses [7]. Oxidative stress is linked to a variety of cardiovascular issues, such as cardiac hypertrophy, atherosclerosis, atrial fibrillation and heart failure [8]. In summary, the generation of free radicals by gamma radiation led to oxidation of macromolecules molecules such as proteins, DNA, and lipids. As a result, protein oxidation products and lipid peroxidation increase, which in turn gives rise to oxidative stress detrimental consequences, including endothelial dysfunction and tissue damage [7]. In the last two decades, investigations on the pathophysiology of radiation-induced cardiotoxicity have increased tremendously, with a particular emphasis on modulation of cellular resistance to oxidants. Nuclear factor erythroid 2-related factor 2 (Nrf2) is a redox-sensitive transcription factor that preserves cellular defense system. It is constitutively expressed in the cytoplasm, and its translocation and activation in the nucleus is favorable in oxidative damage to regulate the transcription of anti-oxidants such as heme oxygenase-1 (HO-1) [9]. An overwhelming body of evidence has revealed that down-regulation of Nrf2 was related to cardiac and vascular complications [10]. Therefore, activating the cellular defense system becomes a key therapeutic target.

Worldwide, statins are typically the medication of choice for patients with cardiovascular disease, especially for those with cancer, where studies have shown a correlation between statins use and survival increase [11, 12]. Rosuvastatin (ROSU) is a reversible inhibitor of 3-hydroxy-3-methylglutaryl coenzyme A reductase (HMG-COA). Although ROSU is therapeutically used to reduce the low-density lipoprotein cholesterol (LDL-C), it also showed a potential effect in mitigating cardiac harm through controlling the oxidative/ nitrosative stress status, as well as suppression of apoptotic and inflammatory markers [13-15].

Oral administration is widely preferred by patients due to its convenience and the ability to sustain an optimal therapeutic concentration in human blood for extended periods of treatment [16]. However, certain drugs with low solubility face challenges in gastrointestinal tract (GI) absorption, necessitating more repeated dosing. For instance, ROSU calcium, with an absolute bioavailability of 20% [17], experiences low water solubility, delayed dissolution, limited permeability, and undergoes hepatic metabolism through oxidation, glucuronidation, and lactonization[18, 19]. As a result, high and frequent drug doses (may be reached three times daily) are required, leading to increased side effects, toxicity, and decreased patient compliance [20]. There is a necessity to design and optimize new formulations to improve ROSU permeability, enhance oral bioavailability, minimize hepatic uptake, and subsequently increase the therapeutic concentration availability.

Bilosomes (BLs) serve as prospective delivery vehicles, which can be employed as drug carriers for oral administration of various medications [21]. As distinguished from traditional vesicles, like liposomes and niosomes, BLs offer preferable characteristics, including limited drug outflow, considerable loading capacity, and efficient transport through the GIT [22]. Various bile salts have been employed in BLs production, acting as permeation enhancers, thereby facilitating BLs transit across biological barriers [23]. They can prevent BLs degradation in GIT, enhancing penetration and improving oral delivery. It was reported that bile salts promote vesicle uptake by intestinal epithelial cells while limiting enzymatic activity at the absorption site [24].

Consequently, this study was designed with a dual focus. The initial phase involves the development of rosuvastatin-loaded bilosomes (ROSU-BLs), evaluating its characteristics as a drug delivery system. Thereafter, the study aims to assess the potential impact of ROSU-BLs versus the free drug form in mitigating radiation-induced cardiovascular damage in experimental rats.

Materials and methods

Materials

Chemicals

Rosuvastatin (ROSU) was a kind gift sample from Hikma Pharmaceuticals Co., 6th October City, Egypt. Two non-ionic surface active agents (SAA); Sorbitanmonostearate (Span 60) was purchased from Merck Schuchardt OHG, Germany. Sorbitanmonopalmitate (Span 40) was obtained from Sigma-Aldrich, Germany. Cholesterol (CHOL), minimum 95% was procured from Panreac, Spain. Deoxycholic acid sodium salt 99% extra pure (SDC) was purchased from Acros Organics Co., Belgium. Chloroform and Methanol (HPLC grade) were obtained from Fisher Chemical, UK.

Methods

Preparation of rosuvastatin loaded bilosomes (ROSU-BLs)

The composition of different developed Rosuvastatin loaded bilosomes (ROSU-BLs) is listed in Table 1. ROSU-BLs were prepared employing the thin film hydration method [25]. In a 100 mL round-bottom flask, precisely measured quantities of ROSU, Span 60 or 40, and CHOL were dissolved in 10 ml chloroform for 10 minutes. The chloroform was gently removed at 56 ± 2 ^{o}C under reduced pressure using a rotary evaporator (VV Micro, Heidolph Instruments GmbH & Co. KG, Germany) for 30 minutes until a dry, thin film was formed on the wall of the flask. Sodium Deoxycholate (SDC) was dissolved in 10 ml phosphate buffered saline (PBS) pH = 7.4, pre-warmed to 56 °C, and then the solution was added to the flask and rotated for 45 minutes to hydrate the thin film to form adispersion of BLs [26, 27]. Small glass beads were used to enhance vesicle yield during hydration [28]. The developed ROSU-BLs were sonicated for 10 minutes using a bath sonicator (Ultra Sonicator, Model LC 60/H Elma, Germany) to reduce the size.

Table 1 Composition and characterization parameters of the developed ROSU-BLs formulations

Formulae	SAA Type	SAA:CHOL:SDC Ratio	EE (%)	PS (nm)	ZP (mV)	PDI
ROSU-BLs 1	Span 60	1:1: 0.25	77.06 ±17.06	267.5 ±0.961	-29.8 ±5.33	0.263
ROSU-BLs 2	Span 60	1:1:0.5	86.87 ±12.94	247.4 ±0.947	-31.2 ±7.52	0.296
ROSU-BLs 3	Span 60	2:1:0.25	72.03 ±12.66	311.9 ±1.028	-14.3 ±5.84	0.515
ROSU-BLs 4	Span 60	2:1:0.5	73.68 ±7.82	414 ±1.103	-27 ±5.93	0.555
ROSU-BLs 5	Span 40	1:1:0.25	69.38 ±14.63	250.3 ±0.915	-30.1 ±8.74	0.33
ROSU-BLs 6	Span 40	1:1:0.5	70.85 ±17.08	252 ±0.935	-27.2 ±5.45	0.321
ROSU-BLs 7	Span 40	2:1:0.25	65.68 ±15.6	251.8 ±0.938	-30.4 ±8.08	0.342
ROSU-BLs 8	Span 40	2:1:0.5	65.47 ±14.81	256.9 ±0.945	-24.8 ±8.49	0.34

* All results are measured as triplicates representing mean ± SD

In vitro characterization and optimization of ROSU-BLs

Drug entrapment efficiency percent (EE %)

To assess the quantity of ROSU entrapped in the developed BLs, the unentrapped ROSU was isolated from the ROSU-BLs through centrifugation at 7000× g and 4 °C using a refrigerated centrifuge (Union 32R, Hanil Co., Korea) for 30 minutes. The resulting pellets were subsequently washed once with PBS (pH = 7.4) for 30 minutes. The washing process was carried out to ensure the thorough removal of any unentrapped ROSU from the loaded BLs. Supernatants were collected and passed through a 0.22 nm Millipore filter (Millipore, USA). The quantity of unentrapped ROSU was determined in the supernatant using a spectrophotometric assay, utilizing UV−Vis recording spectrophotometer (UV-2401 PC, Shimadzu Co., Japan) set to measure absorbance at 242 nm. The measurements were done in triplicate; the percentage of drug entrapment efficiency, expressed as EE%, was calculated as follows:

EE%= [(Total amount of ROSU added - Amount of unentrapped ROSU)/ Total amount of ROSU] X 100

Particle size, polydispersity index and zeta potential analysis

Particle size (PS), polydispersity index (PDI), and zeta potential (ZP) analysis of the developed ROSU-BLs were determined by dynamic light scattering (DLS) using Zeta-sizer (Nano Series ZS90, Malvern Instruments Ltd., Worcestershire, UK) via a helium-neon laser with wavelength of 633 nm at room temperature. All developed formulations followed adequate sample dilution 1:100 (v/v) [25, 29] with double distilled water. All measurements were estimated as an average of three independent samples (±SD).

Selection of the optimized ROSU-BLs

A comparison among all prepared ROSU-BLs formulations was conducted to assess and select the optimal formulation based on the EE%, PS, and ZP values. Subsequently, the chosen formula underwent further investigation.

Characterization of the optimized formulations

Transmission electron microscopy (TEM)

The optimized formulation's morphological features were examined using TEM (JEOL Co., JEM-2100, Japan). One drop of the diluted sample, at 1:100 (v/v), the sample was dropped on a carbon-coated copper grid and allowed to air dry for 15 minutes at room temperature for staining. Subsequently, the grid was sprayed with a drop of 1%w/v phosphotungstic acid solution and left to stand for 3 minutes before being inserted into the microscope. The samples were then examined for surface features and shape at various magnifications power.

Fourier transform infrared (FT-IR) spectroscopy analysis

The potential chemical interaction among the components of the selected ROSU-BLs was identified through FT-IR analysis using an FTIR spectrophotometer (JASCO 6100, Tokyo, Japan). Span 60, SDC, ROSU, and freeze-dried optimized ROSU-BLs 2 were individually combined with KBr and compressed at a pressure of 200 kg/cm^2 for 2 minutes using a hydraulic press to produce the pellets. Each KBr pellet containing the sample was then scanned against a blank KBr pellet background within the wave number range of 4000−400 cm^{-1}.

X-ray powder diffraction (XRPD)

Samples of ROSU, Span 60, CHOL, SDC, optimized ROSU-BLs 2, and physical mixtures (approximately 200 - 300 mg each) were analyzed using X-ray powder diffraction(XRPD). Diffraction patterns wereobtained using the X-ray powder diffractometer (PANalytical EMPYREAN, UK). The X-ray generator was operated at 45 kV tube voltages and 30 mA tube current, utilizing

the Ka lines of copper as the radiation source. The diffraction angle ranged from 4 to 80° of (2θ) range in the step scan mode with a step size of 0.026° (2θ) and a step time of 21.42 s.

In vitro release study of the optimized ROSU-BLs

The study of the in-vitro release behavior of ROSU from BLs was conducted in 0.1N HCl (pH 1.2) and phosphate buffer saline (PBS) (pH 6.8) using the dialysis bag method to simulate gastric and small intestine pH mediums [30, 31]. For this investigation, 2 mg equivalents of the BLs formulation and aqueous suspension of ROSU were placed in dialysis bags (Dialysis tubing cellulose membrane, Sigma Co., USA; molecular weight cutoff 12,000−14,000) [27]. To prevent drug outflow, the bags were sealed on both ends before being suspended in 100 ml screw-capped glass containers filled with one of the release media to maintain sink condition [32]. The experiment was conducted at (37 ± 0.5°C) in a thermo-stated shaking water bath (Memmert, SV 1422, Germany) shaken at 100 rpm. Samples were withdrawn at fixed time intervals (0.5, 1, 2, 3, 4, 5, 6, 7, 8, and 24 hours) and replaced with an equal volume of fresh release medium. The spectrophotometric analysis of ROSU concentrations in the withdrawn samples was conducted by comparison to a blank sample treated in the same conditions. The release percentages were calculated by dividing the amount of drug released by the initial amount of drug in the dialysis bag. All measurements were conducted in triplicate using three separate samples.

Various mathematical models were used for kinetic analysis of drug release from the optimized BLs vesicles, like zero and first-order kinetic models [33], Higuchi's square root of time model [34] and Peppas exponential equation [35]. The coefficient of determination (R2 values) was calculated from the plots Q vs. t in case of zero order, log (Q0 - Q) vs. t for first order, Q vs. t1/2 for Higuchi model, and (log Q vs. log t) for Peppas equation. Where(Q) is the percentage of the released drug at a time (t) and (Q0 - Q) is the remaining percentage of the drug after time (t). In Peppas model, the release exponent "n" was calculated to suggest drug release mechanism.

In vivo study

Animals

Female Wistar rats (weighing 150-200 gm), were taken from the animal breeding facility of the National Centre for Radiation Research and Technology (NCRRT). Animals were adapted for at least one week before experiment in the animal facility of NCRRT at a temperature of 25±1 °C, humidity of 60±5% and natural lighting conditions. They were given free access to a standard pellet diet and water ad libitum.

Ethics approval

All animal experiments complied with the Animal Research Reporting of In Vivo Experiments (ARRIVE) guidelines and were carried out in accordance with the National Research Council's Guide for the Care and Use of Laboratory Animals (NIH publications No. 8023, revised 1978). The in vivo study and all the methods were performed according to the guidelines set by the Research Ethics Committee at the NCRRT (permit number: 10A/ 24).

Irradiation

Rats were exposed to acute whole-body gamma (γ)-radiation at a dose level of 7 Gy [36]. Irradiation was performed up at the NCRRT employing the Gamma Cell-40 biological irradiator with a Caesium^{137} source (Atomic Energy of Canada Ltd; Sheridan Science and Technology Park, Mississauga, Ontario, Canada). The dosage rate during the experiment was 0.33 Gy/min.

Experimental design

A set of 30 rats were adapted for one week preceding the experiment, then they were distributed at random into 5 groups (n=6) as follows: Normal: received bi-distilled water and served as negative control group, IR: rats were irradiated at 7 Gy and received oral bi-distilled water. This group served as positive control, Drug-free BLs: irradiated rats received daily 1 ml drug-free bilosomes, Free ROSU: irradiated rats received daily treatment of free rosuvastatin at a dose of 10 mg/kg [37], ROSU-BLs: irradiated rats treated with rosuvastatin-loaded bilosomes on a daily basis at the same dose of free drug.

On the first day, irradiation of rats was carried out and all treatments were orally administered once daily for 7 days, starting immediately after radiation exposure. At the end of experiment (on the 8th day), all animals were anesthetized using ketamine (80 mg/kg, i.p.) then scarified by cervical dislocation, and blood samples were collected via decapitation for estimation of lipid profile. The heart tissues were rapidly excised, rinsed with ice-cold saline in Petri dishes, and divided into two portions; one portion was embedded in 10% formaldehyde for histopathological examination, and another portion was homogenized in ice-cold phosphate buffersaline to prepare 20% homogenates, which were centrifuged at 4000 rpm at 4 ºC for 10 min. The supernatants were then distributed into several aliquots and stored at -80 ºC to be employed for biochemical tissue analysis.

Assessment of serum lipid profile

Serum levels of total cholesterol, triglycerides, low density lipo-protein (LDL) and high density lipo-protein (HDL) were measured using particular colorimetric test kits (Biodiagnostic Co., Egypt) and following the manufacturer's instructions. The values were given as mg/dl.

Assessment of redox state biomarkers

Estimation of Nrf2 and HO-1 concentrations in heart homogenate was carried out by ELISA technique using rat Nrf2 kit (Cat# EK720003, AFG Bioscience®, Northbrook, IL, USA) and rat HO-1 kit (Cat# E-EL-R0528, Elabscience®, Texas, USA).

Assessment of inflammatory and apoptotic biomarkers

Estimation of tumor necrosis factor-alpha (TNF-α) and caspase-9 concentrations in heart homogenate was carried out by ELISA technique using rat TNF-α kit (Cat# ER1393, Wuhan Fine Biotech Co., Ltd, Wuhan,

China) and rat caspase-9 kit (Cat# SL0154Ra,SunLong Biotech® Co., Ltd, Hangzhou, China).

Histopathological examination

Heart tissue specimens were preserved in 10% neutral buffered formalin, then cut, washed, and dehydrated inincreasing concentrations of alcohol. The dried specimens were cleared in xylene, fixed in paraffin blocks, and sliced at 4-6 µm thickness. The obtained tissue slices were deparaffinized with xylol and stained with haematoxylin and eosin (H&E) for histological analysis under an electric light microscope.

Statistical analysis

Data were expressed as mean ± standard error (SEM). Statistical analysis was carried out using one-way analysis of variance (ANOVA) tests followed by the Tukey multiple comparison post-hoc tests. GraphPad Prism® software package, (GraphPad Software Inc., San Diego,California, USA) was used to carry out all statistical tests. A *p*-value of less than 0.05 was considered significant.

Results and discussion

Preparation of ROSU-BLs

In the present study, ROSU-BLs were formulated employing the thin film hydration method. Table 1 contains the composition of a total of eight prepared formulations, and the results of EE%, PS, ZP, and PDI, where BLs were successfully formed with both molar ratios.

Characterization of the prepared ROSU-BLs

Determination of encapsulation efficiency (EE%)

Results of EE% for the prepared formulations are presented in Table 1. Each formulation presented favorable EE% values, varying from 65.47 ±14.81% to 86.87 ±12.94%. This high EE% could be attributed to the relatively hydrophilic feature of ROSU, as the aqueous solubility of ROSU is 5.40 x 10^{-6} [38], where the drug has been demonstrated to exhibit a higher affinity for vesicle bilayers when using lipophilic surfactants [39, 40]. It was noted that the EE% values were elevated in the case of BLs prepared with Span 60, which possesses higher lipophilicity (HLB: 4.7), compared to BLs prepared with Span 40 (HLB: 6.7) under the same drug quantities and SAA:CHOL ratios.

Also, the CHOL concentration increase leads to an increase in EE%. This effect may be attributed to the enhancement of membrane rigidity and the strengthening of lipid bilayer solidity, and these were reflected in improved permeability, stabilized structure, and prevention of drug leakage from BLs [41]. The incorporation of specific bile salts, such as sodium deoxycholate (SDC), enhances the BLs colloidal stability, allowing them to withstand the disruptive effects of biological acids in the GIT [42]. Furthermore, the elevation of the bile salts ratio from 0.25 to 0.5 resulted in a proportional increment in the EE% of ROSU. This could be returned to the surface-active characteristics of bile salts that are presumed to integrate vertically into the surface of bilayer membrane, disrupt the lipid matrix acyl chains, enhance membrane flexibility, and ultimately improve the solubility of the relatively hydrophilic drug within the membrane [43, 44].

Particle size (PS) and polydispersity index (PDI)

The ROSU-BLs formulations PS analysis results demonstrated that the size of the formulations fell within 247.4 ±0.947 to 414 ±1.103 nm (Table 1), proving that all prepared formulations were in the nanosized scale. In general, the PS is notably smaller when the ratio between SAA:CHOL was 1:1 compared to 2:1, irrespective of the bile salt (BS) ratio used, and this may be due to the impact of CHOL on the physical properties of the vesicles [45]. When cholesterol content is reduced, the lipid bilayer may become more fluid and less rigid, and the increase in fluidity can lead to a looser packing of lipids and result in larger vesicle sizes. While, the increasing of CHOL content enhances the stability of the vesicles by stabilizing the BLs structure and increases the membrane rigidity through the reinforcement of the lipid bilayer membrane solidity [41]. Also, the observed effect of CHOL addition on decreasing particle size can be attributed to the enhancement of bilayer hydrophobicity. This increase in hydrophobicity may reduce the surface free energy, ultimately leading to a decrease in particle size [45-47]. Due to its bulky structure, the increase in SDC content has led to a relatively larger particle size for most of the prepared ROSU-BLs. This has supported the steric stabilization effect, enhancing the stability of the vesicles, preventing aggregation, and maintaining the integrity of the vesicular structure [28, 48].

The polydispersity Index (PDI) results revealed that six formulations exhibited PDI values in the range of 0.2 to 0.4, which can be considered as moderate polydisperse, while two formulations exhibited PDI values more than 0.4 and thus can be considered as polydisperse distribution [49, 50].

Zeta potential (ZP)

Table 1 demonstrated that all ROSU-BLs formulations exhibited negative charges varying from (-14.3 ± 5.84 to -31.2 ± 7.52 mV), signifying stable dispersions. The negative charge of the formulations indicated the deposition of bile salts within the phospholipid bilayer of the developed BLs, increasing the negative surface charge [49]. The ZP values intensified in proportion to the bile salts amount, suggesting the integration of bile salts within the lipid bilayer [49, 51]. The presence of the carboxylate group within the SDC side chain was the factor accountable for enhancing the charge intensity on BLs. This finding aligns with Mazer's concept, suggesting that bile salt molecules were integrated into the BLs layers rather than solely being adsorbed on the vesicular surface [52].

Selection of the optimized ROSU-BLs

Based on the data provided in Table 1 for EE%, PS, and ZP for all prepared BLs formulations, ROSU-BLs 2 demonstrated the highest significant EE% (86.87% ±12.94), with reduced PS (247.4 nm ±0.947) and a ZP of (-31.2 mV ±7.52). These results indicate that ROSU-BLs 2 can be identified as the optimized formula, and further characterization was conducted on it.

Characterization of the optimized ROSU-BLs

Transmission electron microscopy (TEM)

The morphology of the optimized ROSU-BLs 2 was depicted in Figure 1. The micrograph revealed that the vesicles exhibited a nearly entire sphere-like shape, appeared in dispersed clusters, and its structure, including their outline and core, is well maintained.

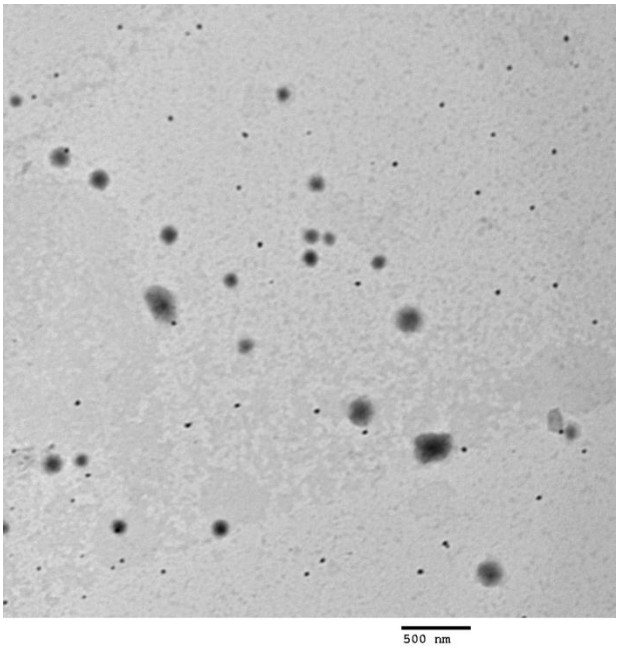

Fig. 1 TEM micrograph of ROSU-BLs 2 formulation stained with 1% phosphotungstic acid.

Fourier transform infrared spectroscopy analysis (FT-IR)

Fourier-transform infrared (FT-IR) spectroscopy is widely reported as a powerful analytical tool for specifying distinctive functional groups and for determining changes within specific fingerprinting regions [53]. FT-IR was performed to study the interaction between of ROSU with different components of BLs. The FT-IR spectra of Span 60, SDC, and the optimized formulation ROSU-BLs 2 were shown in Figure 2. The pursue spectra were realized at a wavenumber varying between 4,000 and 650 cm^{-1} [54].

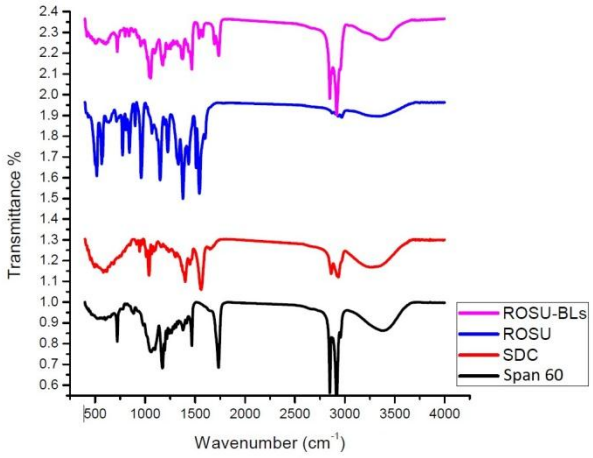

Fig. 2 FTIR thermos grams of ROSU-BLs formulation and individual components.

In brief, Span 60 spectra showed distinctive peaks of 2920 cm^{-1}, and 2921 cm^{-1}, which verify the carboxylic acid functional group. FT-IR spectrum of SDC showed distinctive peaks at 1300 cm^{-1}, 1562 cm^{-1}, 2863.3 cm^{-1}, and 2935.9 cm^{-1}, where C-H and COO- stretching vibration band appear [55]. FTIR analysis of pure ROSU showed characteristic peaks at 3337.90 cm^{-1}, 2968 cm-1, 1599.49 cm^{-1}, 1543.09 cm^{-1}, 1509.24 cm^{-1},1379.23 cm^{-1} and 1150.88 cm^{-1}. These are almost the same as reported in the monograph for ROSU, maintaining the official limits (±100 cm^{-1}). These readings correspond to cyclic amines C-H stretching, C=O stretching, and O-H bending.

The IR spectrum of the optimized ROSU-BLs 2 exhibited minor shifts and reduced intensity in the characteristic peaks of ROSU. These alterations could be related to the occurrence of physical interactions between ROSU and other BLs components, such as Van der Waals bonds, hydrogen bonds, or dipole interactions. Also, it is important to confirm that no chemical changes in the structure of ROSU occurred after encapsulation, which helped in providing suitable and optimal conditions for entrapment of ROSU within the BLs [56]. It is reasonable to clarify that the molecular structure of ROSU remained unchanged and that its functionality was preserved within the encapsulated formulations. The slight differences in intensities suggest that ROSU was effectively encapsulated in the BLs [57].

X-ray powder diffraction (XRPD)

X-ray powder diffraction (XRPD) is one of the most important parameters for studying changes that may occur in the polymorphic characteristics of certain compounds [58], since many active pharmaceutical ingredients (APIs) can be found in various solid-state forms such as polymorphs or amorphous states, and these different solid forms can vary significantly in their physicochemical properties and may potentially influence the efficacy of the drug product. Therefore, the physical state of ROSU-BLs 2 formulation and pure individual components were assessed by XRPD analysis to investigate their crystallinity, as shown in Figure 3. The XRPD of pure ROSU revealed a broad peak at an angle of 20° with scattered angles at 6.8, 21.6, and 24.2, which indicated the semi-crystalline nature of the drug [59].

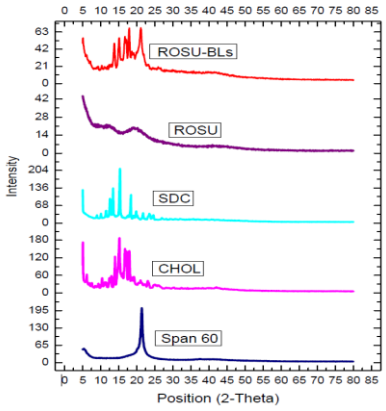

Fig. 3 XRD spectra of ROSU-BLs 2 formulation and pure component (ROSU, SDC, CHOL, Span 60).

The disappearance of ROSU documented peak observed in ROSU-BLs XRPD diffractogram (Figure 3) indicates a reduction in the degree of crystallinity and may be the crystalline state has been entirely transformed into an amorphous state, resulting in improved encapsulation efficiency [59].

In vitro release study

In vitro release studies are often performed for several reasons, including assessing drug availability during preliminary investigations and identifying critical factors that may impact bioavailability. The release of the drug from the vesicles is a crucial factor that significantly determines the pharmacological performance of the dosage form [60]. Any drug cannot exert a therapeutic effect while it is encapsulated, and any type of vesicle needs to maintain the drug in a stable state until it reaches the target site and then promptly release its drug to reach the optimal therapeutic concentration [60].

The release profile of ROSU from the optimized ROSU-BLs 2 formulation and the plain ROSU suspension is depicted in Figure 4. This study was conducted in two release media: 0.1 N HCl (pH 1.2) and PBS (pH 6.8), replicating the pH gradient of the gastrointestinal tract. With both media, ROSU release from the ROSU-BLs formulation exhibited a biphasic pattern. Initially, there was a rapid to moderate release phase, where over 50% of the entrapped ROSU was released from the BLs during the first 4 hours. This slightly rapid release phase may be attributed to the discrete ROSU located on the outer surface of the BLs, and subsequently, the gradual release of ROSU from the incorporated drug inside the bilayers of the BLs [61, 62]. The sustainable release behavior from the BLs dispersions, which followed the initial phase and extended up to 24 hours, may refer to the characteristics of BLs as vesicles, serving as drug reservoirs capable of releasing encapsulated drugs in an extendable controlled manner [63].

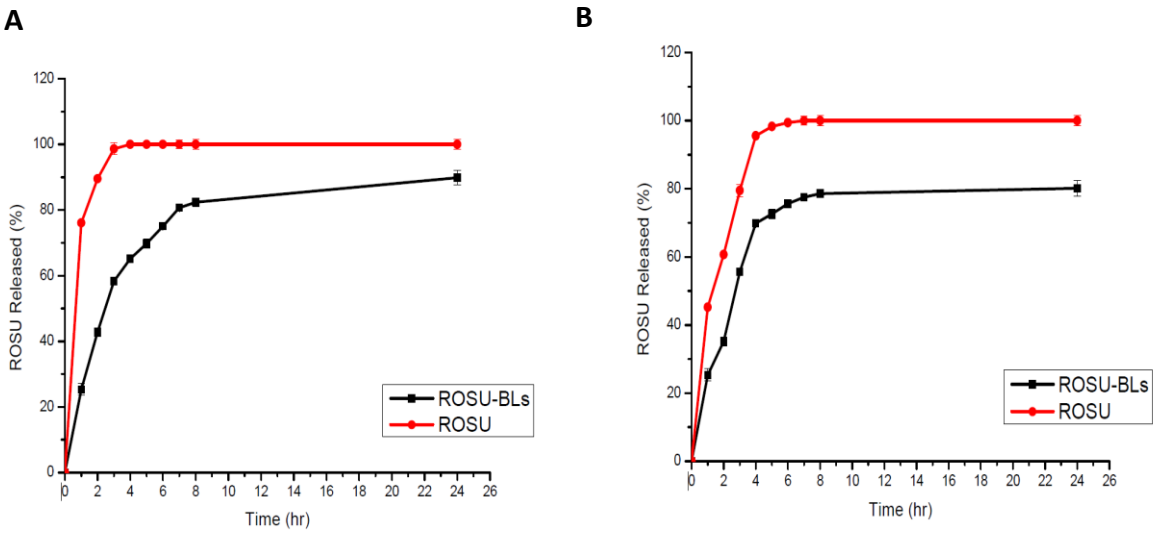

Fig. 4 Release profiles of ROSU from ROSU-BLs 2 formulation and free ROSU suspension in (A) 0.1N HCl (pH 1.2) and (B) PBS (pH 6.8).

Linear regression analysis of the mathematical models was employed for ROSU release data from Free ROSU suspension and from the optimized ROSU-BLs 2 formulation for both release mediums is shown in Table 2. When compared to different kinetic models, the results showed that the correlation coefficient (R^2) values of ROSU as well as ROSU-BLs demonstrated a better fit with Higuchi's model. The Peppas equation was employed to further examine the ROSU release mechanism. This analysis revealed good linearity, while n value indicated that the diffusion complied with an anomalous (non-Fickian) diffusion pattern [64-66].

Table 2 The calculated correlation coefficients and kinetics parameters of ROSU releaseprofile from the optimized ROSU-BLs 2 formulation and plain drug suspension.

Code	Q_{8h} ± SD (%)	Zero Order	First Order	Higuchi	Peppas	
		R^2			R^2	N
ROSU in HCL	100±2.54	0.0950	**0.0919**	0.1839	0.5547	0.2833
ROSU-BLs 2 in HCL	75.03±3.26	0.4998	0.3423	0.6617	0.7952	0.1715
ROSU in PBS	98.30±1.23	0.1450	0.1340	0.2601	0.7382	0.2330
ROSU-BLs 2 in PBS	75.64±0.56	0.4971	0.3374	0.6394	0.7735	0.1642

Q_{8h}: Percent total ROS released after 6 h.

In vivo results

While the use of radiotherapy in cancerous tumors is becoming more prevalent, the dangers must be carefully considered;exposure to radiation has garnered significant emphasis on the cardiovascular tissue, asirradiation has been shown to adversely affect heart tissue, increasecardiac complications,and eventually cause cardiac malfunction, which would urge restricting the dose and usage of radiotherapy in cancer patients[5, 67].Clinical studies showed profits of ROSU against cardiac toxicity in cancer patients receiving either chemotherapy or radiotherapy [68, 69]. Previously, it was clearly demonstrated that acute exposure of experimental animals to gamma radiation at different dosage levels (ranging from 6 to 8 Gy) caused disturbances in cardiac functions with subsequent alterations increatine kinase, and lactate dehydrogenase activities, as well as troponin content [70-72]. Therefore, the current study was conducted to investigate the potential cardiovascular protective effect of ROSU-BLs, and compare its effect with the same dose of free drug form in experimentally irradiated rats.

Herein, the detrimental effect of radiation exposure on the cardiovascular tissue was first assessedby histopathologicalanalyses, as shown in Figure 5 and Table 3. Examination of the cardiac tissue section of the normal group revealedproperly organized cardiac muscle with elongated branching cardiac bundles, which exhibited rounded vesicular centrally located nuclei. The pericardium region covered by intact mesothelial cells was seen. No pathological changes, including necrosis, edema, and inflammation,had been recorded (-). The coronary arterial branches consisted histologically of separate layers of tunica intima, internal elastic lamina, tunica media (several layers of smooth muscle)and external elastic lamina (multiple layers),that extended into tunica adventitia(Figure 5A).

Table 3 Histopathological assessment of heart tissues from various experimental groups

Groups	Necrosis	edema	Inflammation
Normal	−	−	-
Irradiated (IR)	++	++	+
IR + Drug Free BLs	++	++	+
IR + Free ROSU	+	++	+
IR + ROSU-BLs	-	+	-

Rats (n = 6) exposed to γ-radiation (7 Gy) and received all treatments for 7 days, started immediately after irradiation. Free ROSU and ROSU-BLs were orally administered at a dose of 10 mg/kg/day.

The myocardial tissuesectionof IR group showed swelling of cardiac muscle fibers with focal areas of coagulative necrosis,which appeared as deeply homogenous eosinophilicpatches (++). Congestion of intra-muscular capillaries as well as areas of blood extravasation was seen. Perivascular mononucleolar cell infiltration, mainly lymphocytes and macrophages, especially around coronary blood vessels (+) and edema between muscle fibers (++) were also observed. Pericardium showed sloughing of mesothelial lining with submesothelialedema and leukocytic infiltration. The coronary branch showed swelling of endothelial lining, which was surrounded by edema and few leukocytic infiltrations (Figure 5B).Such effect was in accordance with an earlier study demonstrating the injurious effect of radiation exposure on the myocardial tissue[73]. In the same direction, myocardial tissuesection of drug free BLs groupprevealed similar histological changes as that shown in IR group (Figure 5C).

Histological sections of free ROSU groupshowed moderate improvement in comparison with previous groups.Cardiac muscle showed moderate edema (++) with few leukocytic infiltration in-between muscular bundles (+). Pericardium appeared intact with small focal necrosis of subepicardial region (+). Thickening of coronary branch wall surrounded by edema was noticed (Figure 5D).Similar effect was demonstrated in the study of Sultan et al., [15], showing that cellular infiltration, interstitial edema and tissue architecture were relatively well preserved in ROSU treated group,in comparisonto disease group. Interestingly, myocardial tissuesection of ROSU-BLs treated group displayed well organised branching muscle fibers split by fine endomysium and contained vesicular centrally located nuclei without necrosis (-) or leukocytic infiltration (-). Epicardium showed mild swelling of mesothelial lining and inter-muscular edema (+). The coronary branch showed normal architecture with mild swelling of endothelial lining (Figure 5E).

Furthermore, the lipid profile was estimated as shown in Table 4. The alterations in lipid profile are considered one of the causal elements that has been strongly linked to the initiation and progression of cardiac harm after radiation exposure. This connection was obviously shown in the current data as γ-irradiation of rats at a dose level of 7 Gy raised the serum total cholesterol, triglycerides, LDL, and VLDL levels, with no alterations in HDL level, as compared to normal group. However, treatment with either ROSU or ROSU-BLs restored these alterations to normal values. The capability of radiation to alter adversely the lipid profile was observed in previous studies, verifying its attribution to cardiovascular damage [36, 74]. This hyperlipidemic state could be attributed to up-regulation of cholesterol biosynthesis following radiation exposure or attributed to the ability of radiation to induce disturbance in LDL cholesterol receptors, resulting in lipid accumulation with subsequent induction of lipid peroxidation [75].

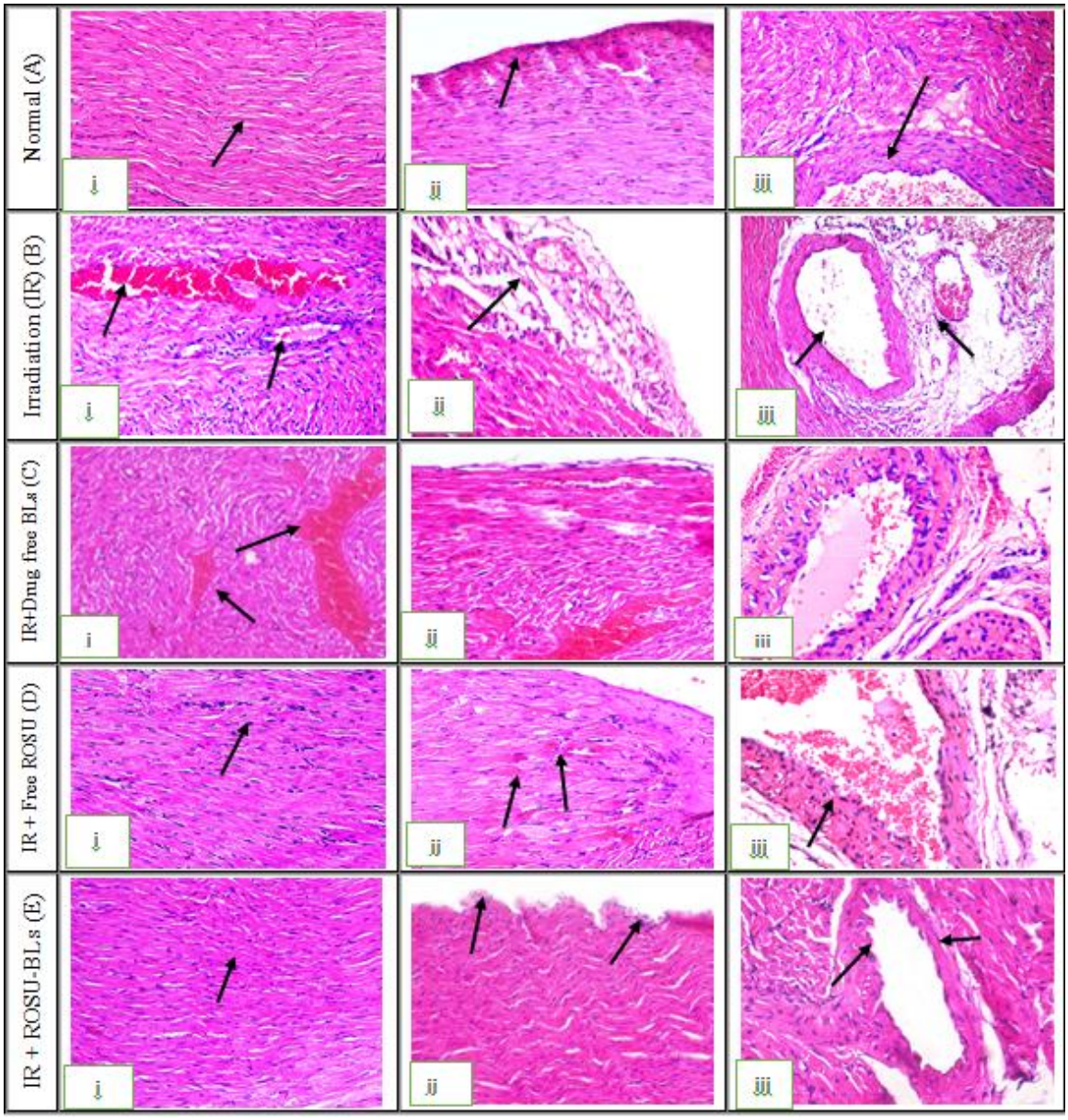

Fig. 5 Photomicrographs of myocardioum tissues of: **(A) Normal** group showing (i) well organized cardiac muscle with elongated branching bundles (ii) intact pericardial mesothelial lining (iii) normal histological structure of coronary branch, **(B) Irradiated (IR)** group showing (i) congestion of intra-muscular capillaries with blood extravasation (ii) sub mesothelial edema and leukocytic infiltration (iii) peri-coronary edema and few leukocytic infiltrations, **(C) IR + Drug Free BLs** group showing (i) muscular necrosis appeared as deeply eosinophilic area (ii) subepicardialoedema with blood extravasation (iii) peri-coronary edema and few leukocytic infiltration, **(D) IR + Free ROSU** group showing (i) moderate edema with few leukocytic infiltration in-between muscular bundles (ii) small focal necrosis of subepicardial region (iii) mild swelling of coronary endothelial lining, **(E) IR + ROSU-BLs** group showing (i) well organized branched muscle fibers (ii) mild swelling of mesothelial lining of epicardium (iii) normal architecture of coronary branch with mild swelling of endothelial lining (H&EX200).

Table 4 Lipid profile of irradiated rats treated with rosuvastatin either in free form or loaded in bilosomes.

Groups	Total cholesterol (mg/dl)	Triglycerides (mg/dl)	LDL (mg/dl)	HDL (mg/dl)	VLDL (mg/dl)
Normal	55.97± 2.89	59.01± 7.60	32.92 ± 2.25	35.12± 3.50	11.80± 1.52
Irradiated (IR)	98.35[a]± 3.64	101.8[a]± 6.16	70.50[a]± 5.82	32.41± 2.76	20.36[a]± 1.23
IR + Drug Free BLs	100.80[a]± 2.56	97.30[a]± 5.51	61.15[a]± 3.90	31.90± 3.23	19.46[a]± 1.10
IR + Free ROSU	73.48[b]± 7.887	49.55[b]± 5.48	43.73[b]± 5.79	35.27± 3.44	9.91[b]± 1.096
IR + ROSU-BLs	67.85[b]± 6.471	44.37[b]± 3.55	37.83[b]± 4.12	36.19± 3.23	8.87[b]± 0.71

Rats (n = 6) exposed to γ-radiation (7 Gy) and received all treatments for 7 days,started immediately after irradiation. Free ROSU and ROSU-BLs were orally administered at a dose of 10 mg/kg/day.Values are represented as mean ±S.E.M. Significant difference ($p< 0.05$) against Normal group represented as (a), significant difference ($p< 0.05$) against IR group represented as (b), significant difference ($p< 0.05$) against IR+Free ROSU group represented as (c). One-way ANOVA was carried using Graph pad prism software followed by Tukey' s Multiple Comparisons test.

The damaging effect of radiation in biological systems is mediated mainly through production of reactive oxygen species (ROS). This elicits an imbalance between pro-oxidant/anti-oxidant, leading to oxidative stress, which causes the oxidation of macromolecules including DNA, proteins, and lipids. As a consequence, protein oxidation and lipid peroxidation products increase and give rise to deleterious consequences of tissue damage [7]. It is noteworthy that improving the redox state of the myocardial cells was an important target for many treatments aimed for hindering the oxidative stress-deteriorating effects. Therefore, the current study considered Nrf2/HO-1 axis as one of the pivotal pathways that maintains cellular redox homeostasis. Nrf2 is a redox-sensitive gene transcription element that controls the gene expression of anti-oxidants in cells. In regular physiological status, Nrf2 is confined inside the cytoplasm by its repressor, Kelch-like ECH associated protein (Keap1). Upon stimulation, Nrf2 detached from its cytoplasmic inhibitor protein and then translocate into the nucleus to activate transcription of anti-oxidant enzymes, including HO-1, NADPH, ferritin, and other anti-oxidant genes, and hence caused cells protection. HO-1 is a major target gene for Nrf2; it is an inducible isoform and rate-limiting enzyme that promotes the degradation of haem into carbon monoxide, biliverdin, and iron, which are crucial endogenous defensive molecules of the body [76].

The current results showed a significant suppression in the myocardial Nrf2 concentration of the IR group by 39% (Figure 6A), and consequently, a marked reduction in the HO-1 level by 61% was also observed (Figure 6B), as compared to normal group ($p< 0.001$). Such results were not expected, but they agreed with previous studies, attributing the disturbance of Nrf2 system to the sustained exposure to γ-radiation; production of ROS may activate Nrf2 to promote anti-oxidant response element-dependent gene expression, but with aggravated exposure to oxidative stress and sustained elevation of ROS, a reduction in Nrf2 levels was found [37, 77]. Herein, the concentration of Nrf2 is highly restored in the ROSU-BLs treated group, as it increased by 36%, compared to IR group ($p< 0.05$), and a slight rise was detected in free ROSU treated group, yet it was not significant (Figure 6A). Whereas, either administration of free ROSU or ROSU-BLs up-regulated the HO-1 protein concentration in heart by 90% and 96%, respectively, as compared to the IR group ($p< 0.05$) (Figure 6B). Interestingly, ROSU has been shown to activate the Nrf2 /HO-1 pathway and promote myocardial cells survival in previous research [78]. Statins had an advantageous impact on Nrf2/HO-1 pathway, as they significantly boosted Nrf2 DNA-binding capacity and stimulated the transcription of its target genes, shielding cells from the ROS damaging effects [79].

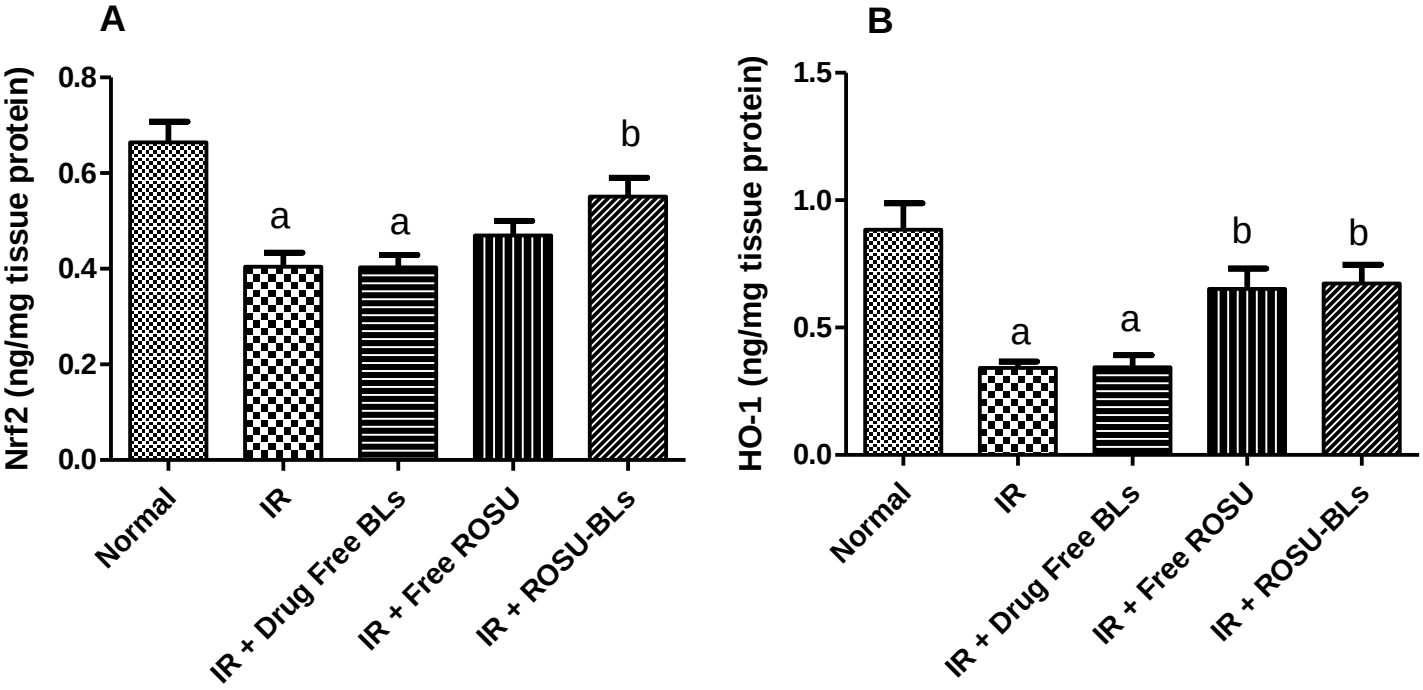

Fig. 6 Effect of ROSU (10 mg/kg) oral administration either in free form or loaded bilosomes on the (A**) Nrf2** and **(B) HO-1** concentrations in cardiac tissue of irradiated rats. Rats (n=6) exposed to radiation (7 Gy) and received treatments for 7 days, started immediately after irradiation. Values are represented as mean ±S.E.M. Significant difference ($p < 0.05$) against Normal group represented as (a), significant difference ($p < 0.05$) against IR group represented as (b), significant difference ($p < 0.05$) against IR+Free ROSU group represented as (c).

In addition to producing direct cell damage, oxidative stress may also function as a second messenger that activates expression of pro-inflammatory cytokines and apoptotic markers.TheROS extensively stimulates tissue resident macrophages to produce inflammatory cytokines such as TNF-α. The activation of TNF-α receptor further activates the nuclear factor-kappa B (NF-κB), a transcription factor, which binds to promoter regions of its target genesand induce transcription of correspondinggenes related toinflammation (7). In particular, Nrf2 as well as HO-1 and its catalytic products play a pivotal role inmodulating inflammation and apoptosis [80, 81]. As shown in Figure 7A, the level of TNF-α was estimated in the current study as an inflammatory marker where exposure to radiation induces a nearly 7-fold increase in the TNF-α cardiac content,as compared to normal group ($p<0.001$). TNF-α is a key mediator in cardiovascular diseases, causing contractile failure, apoptosis, and activating other inflammatory cytokines [82]. Notably, oral administration of free ROSU suppressed the TNF-α by 28% ($p<0.01$), whereas treatment with ROSU-BLs repressed the TNF-α by 55% ($p<0.001$) and exhibited a significant difference from the free ROSU by 37% ($p<0.01$), thus indicating the patent effect of ROSU-BLs.The ability of ROSU to mitigate the rise of TNF-α was in consistent with previous study reporting its cardioprotective impact against myocardial injury through suppression of TNF-α and upregulation of Nrf2 [15].

Downstream to inflammatory response, apoptosis and necrosis were activated [82], which are the main modes of cell death associated with radiation-induced cardiac injury. In this context, the level of caspase-9 was assessedin the present study as apro-apoptotic marker (Figure 7B). Exposure to radiation induced a significant rise in caspase-9 level by 32%, as compared to normal group ($p<0.05$). Treatment with free ROSU led to non-significant suppression in caspase-9 contentby 21%, whereas administration of ROSU-BLs induced a significant suppression in the caspase-9 content by 26%, as compared to IR group ($p<0.01$). The anti-apoptotic potential of ROSU was previously verified in an in-vitro studyof Wang et al., [83]that showed the significance of ROSU in suppressingthe expression of caspase-3 and caspase-9. As a conclusion, the current results demonstrate the efficacy of bilosomes carrier in improving the oral delivery of ROSU, evidenced by the enhanced potential of ROSU-BLs to alleviate cardiovascular impairment caused by radiation. The results also showed the substantial impact of ROSU-BLs in activating the cardiac redox status via activating Nrf2/HO and its superiority in suppressing the inflammatory and apoptotic markers.

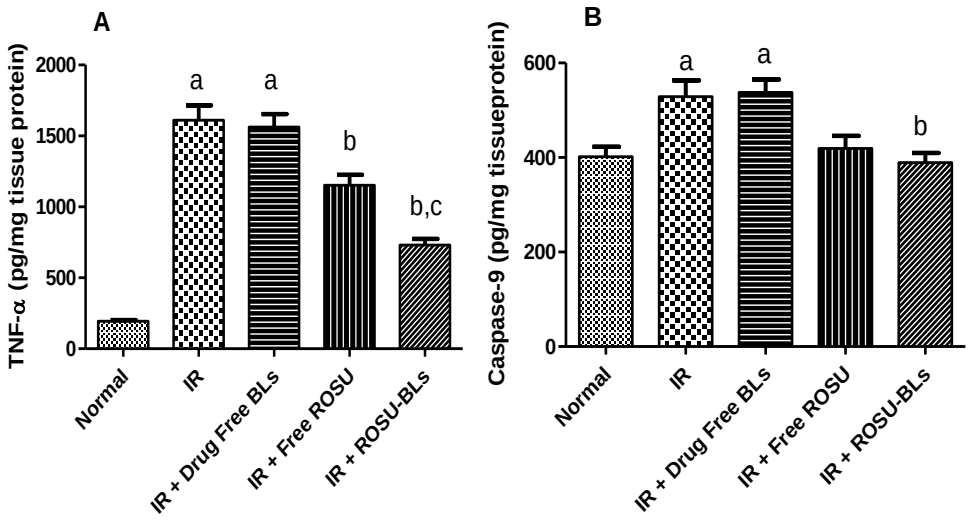

Fig. 7 Effect of ROSU (10 mg/kg) oral administration either in free form or loaded bilosomes on the **(A) TNF-α** and **(B) Caspase-9** concentrations in cardiac tissue of irradiated rats. Rats (n = 6) exposed to radiation (7 Gy) and received treatments for 7 days, started immediately after irradiation. V are represented as mean ±S.E.M. Significant difference ($p < 0.05$) against Normal group represented as (a), significant difference ($p < 0.05$) against IR group represented as (b), significant difference ($p < 0.05$) against IR+Free ROSU group represented as (c).

Conflicts of interest

The authors declare there are no conflicts of interest.

Acknowledgement

The authors wish to acknowledge Dr. Ahmed H. Osman, professor of pathology, Faculty of Veterinary Medicine, Cairo University, for his professional help in carrying out the histolopathological examinations.

References

1. Jacobs JEJ, L'Hoyes W, Lauwens L, Yu YL, Brusselmans M, Weltens C, Voigt JU, Wildiers H, Neven P, Herrmann J, Thijs L, Staessen JA, Janssens S, Van Aelst LNL. Mortality and major adverse cardiac events in patients with breast cancer receiving radiotherapy: the first decade. J Am Heart Assoc 2023; 12:e027855.
2. No HJ, Guo FB, Park NJ, Kastelowitz N, Rhee JW, Clark DE, Chin AL, Vitzthum LK, Horst KC, Moding EJ, Loo BW, Jr., Diehn M, Binkley MS. Predicting adverse aardiac events after radiotherapy for locally advanced non-small cell lung cancer. JACC CardioOncol 2023; 5:775-787.
3. Wang JZ, Wang Y, Shao Q, Li JB. Dynamic changes in cardiac biomarkers in radiotherapy for oesophageal cancer and their correlations with cardiac radiation dosimetry. Clin Transl Radiat Oncol 2024; 45:100750.
4. Chang HM, Okwuosa TM, Scarabelli T, Moudgil R, Yeh ETH. Cardiovascular complications of cancer therapy: best practices in diagnosis, prevention, and management: part 2. J Am Coll Cardiol 2017; 70:2552-2565.
5. Puukila S, Lemon JA, Lees SJ, Tai TC, Boreham DR, Khaper N. Impact of ionizing radiation on the cardiovascular system: a review. Radiat Res 2017; 188:539-546.
6. Gkantaifi A, Papadopoulos C, Spyropoulou D, Toumpourleka M, Iliadis G, Kardamakis D, Nikolaou M, Tsoukalas N, Kyrgias G, Tolia M. Breast radiotherapy and early adverse cardiac effects. the role of serum biomarkers and strain echocardiography. Anticancer Res 2019; 39:1667-1673.
7. Ping Z, Peng Y, Lang H, Xinyong C, Zhiyi Z, Xiaocheng W, Hong Z, Liang S. Oxidative stress in radiation-induced cardiotoxicity. Oxid Med Cell Longev 2020; 2020:3579143.
8. Senoner T, Dichtl W. Oxidative stress in cardiovascular diseases: still a therapeutic target? Nutrients 2019; 11:2090.
9. Zhang X, Yu Y, Lei H, Cai Y, Shen J, Zhu P, He Q, Zhao M. The Nrf-2/HO-1 signaling axis: a ray of hope in cardiovascular diseases. Cardiol Res Pract 2020; 2020:5695723.
10. Wang J, Xiao M, Wang J, Wang S, Zhang J, Guo Y, Tang Y, Gu J. NRF2-related epigenetic modifications in cardiac and vascular complications of diabetes

mellitus. Front Endocrinol (Lausanne) 2021; 12:598005.
11. Heiston EM, Hundley WG. Statins for cardiac and vascular protection during and after cancer therapy. Curr Oncol Rep 2022; 24:555-561.
12. Zhou Q, Jiao Z, Liu Y, Devreotes PN, Zhang Z. The effects of statins in patients with advanced-stage cancers - a systematic review and meta-analysis. Front Oncol 2023; 13:1234713.
13. Lv Q, Wang Y, Li Y, Zhao L, Gong Y, Wang M, Wang M, Fu G, Zhang W. Rosuvastatin reverses hypertension-induced changes in the aorta structure and endothelium-dependent relaxation in rats through suppression of apoptosis and inflammation. J Cardiovasc Pharmacol 2020; 75:584-595.
14. Wang P, Luo L, Shen Q, Shi G, Mohammed A, Ni S, Wu X. Rosuvastatin improves myocardial hypertrophy after hemodynamic pressure overload via regulating the crosstalk of Nrf2/ARE and TGF-β/ smads pathways in rat heart. Eur J Pharmacol 2018; 820:173-182.
15. Sultan F, Kaur R, Tarfain NU, Mir AH, Dumka VK, Sharma SK, Singh Saini SP. Protective effect of rosuvastatin pretreatment against acute myocardial injury by regulating Nrf2, Bcl-2/Bax, iNOS, and TNF-α expressions affecting oxidative/nitrosative stress and inflammation. Hum Exp Toxicol 2022; 41:9603271211066065.
16. Li J, Jiang C, Lang X, Kong M, Cheng X, Liu Y, Feng C, Chen X. Multilayer sodium alginate beads with porous core containing chitosan based nanoparticles for oral delivery of anticancer drug. Int J Biol Macromol 2016; 85:1-8.
17. Climent E, Benaiges D, Pedro-Botet J. Hydrophilic or Lipophilic Statins? Front Cardiovasc Med 2021; 8:687585.
18. Karasulu HY, Gundogdu E, Turgay T, Turk UO, Apaydin S, Simsir IY, Yilmaz C, Karasulu E. Development and optimization of self-emulsifying drug delivery systems (SEDDS) for enhanced dissolution and permeability of Rrosuvastatin. Curr Drug Deliv 2016; 13:362-370.
19. Balakumar K, Raghavan CV, selvan NT, prasad RH, Abdu S. Self nanoemulsifying drug delivery system (SNEDDS) of rosuvastatin calcium: design, formulation, bioavailability and pharmacokinetic evaluation. Colloids Surf B Biointerfaces 2013; 112:337-343.
20. Elsayed I, El-Dahmy RM, El-Emam SZ, Elshafeey AH, El Gawad NAA, El-Gazayerly ON. Response surface optimization of biocompatible elastic nanovesicles loaded with rosuvastatin calcium: enhanced bioavailability and anticancer efficacy. Drug Deliv Transl Res 2020; 10:1459-1475.
21. Elkomy MH, Eid HM, Elmowafy M, Shalaby K, Zafar A, Abdelgawad MA, Rateb ME, Ali MRA, Alsalahat I, Abou-Taleb HA. Bilosomes as a promising nanoplatform for oral delivery of an alkaloid nutraceutical: improved pharmacokinetic profile and snowballed hypoglycemic effect in diabetic rats. Drug Deliv 2022; 29:2694-2704.
22. Elkomy MH, Alruwaili NK, Elmowafy M, Shalaby K, Zafar A, Ahmad N, Alsalahat I, Ghoneim MM, Eissa EM, Eid HM. Surface-modified bilosomes nanogel bearing a natural plant alkaloid for safe management of rheumatoid arthritis inflammation. Pharmaceutics 2022; 14.
23. Waglewska E, Pucek-Kaczmarek A, Bazylińska U. Novel surface-modified bilosomes as functional and biocompatible nanocarriers of hybrid compounds. Nanomaterials (Basel) 2020; 10:2472-2485.
24. Aburahma MH. Bile salts-containing vesicles: promising pharmaceutical carriers for oral delivery of poorly water-soluble drugs and peptide/protein-based therapeutics or vaccines. Drug Deliv 2016; 23:1847-1867.
25. Aziz DE, Abdelbary AA, Elassasy AI. Investigating superiority of novel bilosomes over niosomes in the transdermal delivery of diacerein: in vitro characterization, ex vivo permeation and in vivo skin deposition study. J Liposome Res 2019; 29:73-85.
26. Zafar A, Alruwaili NK, Imam SS, Hadal Alotaibi N, Alharbi KS, Afzal M, Ali R, Alshehri S, Alzarea SI, Elmowafy M, Alhakamy NA, Ibrahim MF. Bioactive apigenin loaded oral nano bilosomes: formulation optimization to preclinical assessment. Saudi Pharmaceutical Journal 2021; 29:269-279.
27. Younis MM, Fadel NA, Darwish AB, Mohsen AM. Nanospanlastics as a novel approach for improving the oral delivery of Rresveratrol in lipopolysaccharide-induced endotoxicity in mice. Journal of Pharmaceutical Innovation 2023; 18:1264-1278.
28. Albash R, El-Nabarawi MA, Refai H, Abdelbary AA. Tailoring of PEGylated bilosomes for promoting the transdermal delivery of olmesartan medoxomil: in-vitro characterization, ex-vivo permeation and in-vivo assessment. Int J Nanomedicine 2019; 14:6555-6574.
29. Mostafa DM, Abd El-Alim SH, Asfour MH, Al-Okbi SY, Mohamed DA, Hamed TE, Awad G. Transdermal fennel essential oil nanoemulsions with promising hepatic dysfunction healing effect: in vitro and in vivo study. Pharm Dev Technol 2019; 24:729-738.
30. Kassem AA, Abd El-Alim SH, Basha M, Salama A. Phospholipid complex enriched micelles: A novel drug delivery approach for promoting the antidiabetic effect of repaglinide. Eur J Pharm Sci 2017; 99:75-84.
31. Salama A, Elgohary R, Kassem AA, Asfour MH. Chrysin-phospholipid complex-based solid dispersion for improved anti-aging and neuroprotective effects in mice. Pharm Dev Technol 2023; 28:109-123.
32. Mishra RK, Ahmad A, Kumar A, Vyawahare A, Raza SS, Khan R. Lipid-based nanocarrier-mediated targeted delivery of celecoxib attenuate severity of ulcerative colitis. Mater Sci Eng C Mater Biol Appl 2020; 116:111103.
33. Najib N, Suleiman MS. The kinetics of drug release from ethylcellulose solid dispersions. Drug Development and Industrial Pharmacy 1985; 11:2169-2181.
34. Higuchi T. Mechanism of sustained-action medication. Theoretical analysis of rate of release of solid drugs dispersed in solid matrices. Journal of Pharmaceutical Sciences 1963; 52:1145-1149.

35. Basha M, Abd El-Alim SH, Kassem AA, El Awdan S, Awad G. Benzocaine loaded solid lipid nanoparticles: Formulation design, in vitro and in vivo evaluation of local anesthetic effect. Curr Drug Deliv 2015; 12:680-692.
36. El-Sabbagh WA, Fadel NA, El-Hazek RM, Osman AH, Ramadan LA. Ubiquinol attenuates γ-radiation induced coronary and aortic changes via PDGF/p38 MAPK/ICAM-1 related pathway. Sci Rep 2023; 13:22959.
37. Fahim TM, Mohamed MAE, Abdelrahman SSM, Lotfy DM. Beneficial effect of rosuvastatin therapy on spleen injury induced by gamma irradiation in rats: targeting Nrf2/EPRE Pathway. Dose Response 2023; 21:15593258231179900.
38. Alshora DH, Haq N, Alanazi FK, Ibrahim MA, Shakeel F. Solubility of rosuvastatin calcium in different neat solvents at different temperatures. The Journal of Chemical Thermodynamics 2016; 94:230-233.
39. Kassem AA, Abd El-Alim SH, Asfour MH. Enhancement of 8-methoxypsoralen topical delivery via nanosized niosomal vesicles: Formulation development, in vitro and in vivo evaluation of skin deposition. Int J Pharm 2017; 517:256-268.
40. Vora B, Khopade AJ, Jain NK. Proniosome based transdermal delivery of levonorgestrel for effective contraception. J Control Release 1998; 54:149-165.
41. Patel KK, Kumar P, Thakkar HP. Formulation of niosomal gel for enhanced transdermal lopinavir delivery and its comparative evaluation with ethosomal gel. AAPS PharmSciTech 2012; 13:1502-1510.
42. Arzani G, Haeri A, Daeihamed M, Bakhtiari-Kaboutaraki H, Dadashzadeh S. Niosomal carriers enhance oral bioavailability of carvedilol: effects of bile salt-enriched vesicles and carrier surface charge. Int J Nanomedicine 2015; 10:4797-4813.
43. Sun J, Deng Y, Wang S, Cao J, Gao X, Dong X. Liposomes incorporating sodium deoxycholate for hexamethylmelamine (HMM) oral delivery: development, characterization, and in vivo evaluation. Drug Deliv 2010; 17:164-170.
44. Porter CJ, Charman WN. In vitro assessment of oral lipid based formulations. Adv Drug Deliv Rev 2001; 50 Suppl 1:S127-147.
45. Marianecci C, Di Marzio L, Rinaldi F, Celia C, Paolino D, Alhaique F, Esposito S, Carafa M. Niosomes from 80s to present: the state of the art. Adv Colloid Interface Sci 2014; 205:187-206.
46. Bernsdorff C, Wolf A, Winter R, Gratton E. Effect of hydrostatic pressure on water penetration and rotational dynamics in phospholipid-cholesterol bilayers. Biophys J 1997; 72:1264-1277.
47. Nowroozi F, Almasi A, Javidi J, Haeri A, Dadashzadeh S. Effect of surfactant type, cholesterol content and various downsizing methods on the particle size of niosomes. Iran J Pharm Res 2018; 17:1-11.
48. El-Nabarawi M, Nafady M, Elmenshawe S, Elkarmalawy M, Teaima M. Liver targeting of daclatasvir via tailoring sterically stabilized bilosomes: fabrication, comparative in vitro/in vivo appraisal and biodistribution studies. Int J Nanomedicine 2021; 16:6413-6426.
49. El-Nabarawi MA, Shamma RN, Farouk F, Nasralla SM. Bilosomes as a novel carrier for the cutaneous delivery for dapsone as a potential treatment of acne: preparation, characterization and in vivo skin deposition assay. J Liposome Res 2020; 30:1-11.
50. El Menshawe SF, Aboud HM, Elkomy MH, Kharshoum RM, Abdeltwab AM. A novel nanogel loaded with chitosan decorated bilosomes for transdermal delivery of terbutaline sulfate: artificial neural network optimization, in vitro characterization and in vivo evaluation. Drug Deliv Transl Res 2020; 10:471-485.
51. Ahmad J, Singhal M, Amin S, Rizwanullah M, Akhter S, Kamal MA, Haider N, Midoux P, Pichon C. Bile salt stabilized vesicles (Bilosomes): a novel nano-pharmaceutical design for oral delivery of proteins and peptides. Curr Pharm Des 2017; 23:1575-1588.
52. Hu S, Niu M, Hu F, Lu Y, Qi J, Yin Z, Wu W. Integrity and stability of oral liposomes containing bile salts studied in simulated and ex vivo gastrointestinal media. Int J Pharm 2013; 441:693-700.
53. Yeo LK, Olusanya TOB, Chaw CS, Elkordy AA. Brief effect of a small hydrophobic drug (Cinnarizine) on the physicochemical characterisation of niosomes produced by thin-film hydration and microfluidic methods. Pharmaceutics 2018; 10:185.
54. Abou Taleb S, Darwish AB, Abood A, Mohamed AM. Investigation of a new horizon antifungal activity with enhancing the antimicrobial efficacy of ciprofloxacin and its binary mixture via their encapsulation in nanoassemblies: in vitro and in vivo evaluation. Drug Dev Res 2020; 81:374-388.
55. Yang L, Xu Y, Su Y, Wu J, Zhao K, Chen J, Wang M. FT-IR spectroscopic study on the variations of molecular structures of some carboxyl acids induced by free electron laser. Spectrochim Acta A Mol Biomol Spectrosc 2005; 62:1209-1215.
56. Mazyed EA, Zakaria S. Enhancement of dissolution characteristics of clopidogrel bisulphate by proniosomes International Journal of Applied Pharmaceutics 2019; 11:77-85.
57. Shruthi PA, Pushpadass HA, Franklin MEE, Battula SN, Laxmana Naik N. Resveratrol-loaded proniosomes: Formulation, characterization and fortification. LWT 2020; 134:110127.
58. Shete G, Puri V, Kumar L, Bansal AK. Solid state characterization of commercial crystalline and amorphous atorvastatin calcium samples. AAPS PharmSciTech 2010; 11:598-609.
59. Al-Heibshy FNS, Basaran E, Arslan R, Ozturk N, Erol K, Demirel M. Physicochemical characterization and pharmacokinetic evaluation of rosuvastatin calcium incorporated solid lipid nanoparticles. Int J Pharm 2020; 578:119106.
60. Solomon D, Gupta N, Mulla NS, Shukla S, Guerrero YA, Gupta V. Role of in vitro release methods in liposomal formulation development: challenges and regulatory perspective. AAPS J 2017; 19:1669-1681.
61. Abd El-Alim SH, Kassem AA, Basha M. Proniosomes as a novel drug carrier system for

buccal delivery of benzocaine. Journal of Drug Delivery Science and Technology 2014; 24:452-458.
62. Abd-Elbary A, El-laithy HM, Tadros MI. Sucrose stearate-based proniosome-derived niosomes for the nebulisable delivery of cromolyn sodium. Int J Pharm 2008; 357:189-198.
63. Chilkawar R, Nanjwade B, Nwaji M, Idris S, Mohamied A. Bilosomes based drug delivery system. J. Chem. Appl 2015; 2.
64. Peppas NA, Sahlin JJ. A simple equation for the description of solute release. III. Coupling of diffusion and relaxation. Int J Pharm 1989; 57:169-172.
65. Lokhande AB, Mishra S, Kulkarni RD, Naik JB. Preparation and characterization of repaglinide loaded ethylcellulose nanoparticles by solvent diffusion technique using high pressure homogenizer. J Pharm Res 2013; 7:421-426.
66. Peppas NA. Analysis of Fickian and non-Fickian drug release from polymers. Pharm Acta Helv 1985; 60:110-111.
67. Armanious MA, Mohammadi H, Khodor S, Oliver DE, Johnstone PA, Fradley MG. Cardiovascular effects of radiation therapy. Curr Probl Cancer 2018; 42:433-442.
68. Huang YJ, Lin JA, Chen WM, Shia BC, Wu SY. Statin therapy reduces radiation-induced cardiotoxicity in patients with breast cancer receiving adjuvant radiotherapy. J Am Heart Assoc 2024; 13:e036411.
69. Kettana KM, El-Haggar SM, Alm El-Din MA, El-Afify DR. Possible protective effect of rosuvastatin in chemotherapy-induced cardiotoxicity in HER2 positive breast cancer patients: a randomized controlled trial. Med Oncol 2024; 41:196.
70. El-Hazek RMM, Zaher NH, El-Gazzar MGM, Fadel NA, El-Sabbagh WA. Novel VEGFR2 inhibitors with thiazoloquinoxaline scaffold targeting hepatocellular carcinoma with lower cardiotoxic impact. Sci Rep 2023; 13:13907.
71. Mansour HH, Tawfik SS. Early treatment of radiation-induced heart damage in rats by caffeic acid phenethyl ester. Eur J Pharmacol 2012; 692:46-51.
72. Soliman AF, Anees LM, Ibrahim DM. Cardioprotective effect of zingerone against oxidative stress, inflammation, and apoptosis induced by cisplatin or gamma radiation in rats. Naunyn Schmiedebergs Arch Pharmacol 2018; 391:819-832.
73. Karam HM, Radwan RR. Metformin modulates cardiac endothelial dysfunction, oxidative stress and inflammation in irradiated rats: A new perspective of an antidiabetic drug. Clin Exp Pharmacol Physiol 2019; 46:1124-1132.
74. El-Desouky WI, Mahmoud AH, Abbas MM. Antioxidant potential and hypolipidemic effect of whey protein against gamma irradiation induced damages in rats. Appl Radiat Isot 2017; 129:103-107.
75. S NS, Raviraj R, Nagarajan D, Zhao W. Radiation-induced lung injury: impact on macrophage dysregulation and lipid alteration - a review. Immunopharmacol Immunotoxicol 2019; 41:370-379.
76. Ndisang JF. Synergistic interaction between heme oxygenase (HO) and nuclear-factor E2- related actor-2 (Nrf2) against oxidative stress in cardiovascular related diseases. Curr Pharm Des 2017; 23:1465-1470.
77. Abdel-Magied N, Shedid SM. The effect of naringenin on the role of nuclear factor (erythroid-derived 2)-like2 (Nrf2) and haem oxygenase 1 (HO-1) in reducing the risk of oxidative stress-related radiotoxicity in the spleen of rats. Environ Toxicol 2019; 34:788-795.
78. Baraka SA, Tolba MF, Elsherbini DA, El-Naga RN, Awad AS, El-Demerdash E. Rosuvastatin and low-dose carvedilol combination protects against isoprenaline-induced myocardial infarction in rats: Role of PI3K/Akt/Nrf2/HO-1 signalling. Clin Exp Pharmacol Physiol 2021; 48:1358-1370.
79. Mansouri A, Reiner Ž, Ruscica M, Tedeschi-Reiner E, Radbakhsh S, Bagheri Ekta M, Sahebkar A. Antioxidant effects of statins by modulating Nrf2 and Nrf2/HO-1 signaling in different diseases. J Clin Med 2022; 11:1313-1333.
80. Ahmed SM, Luo L, Namani A, Wang XJ, Tang X. Nrf2 signaling pathway: Pivotal roles in inflammation. Biochim Biophys Acta Mol Basis Dis 2017; 1863:585-597.
81. Wu C, Chen RL, Wang Y, Wu WY, Li G. Acacetin alleviates myocardial ischaemia/reperfusion injury by inhibiting oxidative stress and apoptosis via the Nrf-2/HO-1 pathway. Pharm Biol 2022; 60:553-561.
82. Urschel K, Cicha I. TNF-α in the cardiovascular system: from physiology to therapy. Int J Interferon Cytokine Mediat Res 2015; 9-25.
83. Wang K, Li B, Xie Y, Xia N, Li M, Gao G. Statin rosuvastatin inhibits apoptosis of human coronary artery endothelial cells through upregulation of the JAK2/STAT3 signaling pathway. Mol Med Rep 2020; 22:2052-2062.